The Astrophysical Journal, 980:51 (8pp), 2025 February 10 https://doi.org/10.3847/1538-4357/adabbf

Long-term Evolution of Sco X-1: Implications for the Current Spin Frequency and Ellipticity of the Neutron Star

Abhijnan Kar[1], Pulkit Ojha[2], and Sudip Bhattacharyya[3]
[1] Department of Physical Sciences, Indian Institute of Science Education and Research Berhampur, Vigyanpuri, Ganjam 760003, India; karabhijnan123@gmail.com
[2] Center for Theoretical Physics, Aleja Lotnikow 32/46, 02-668, Warszawa, Poland; pojha@cft.edu.pl
[3] Department of Astronomy and Astrophysics, Tata Institute of Fundamental Research, 1 Homi Bhabha Road, Colaba, Mumbai 400005, India; sudip@tifr.res.in
Received 2024 November 25; revised 2025 January 14; accepted 2025 January 15; published 2025 February 4

Abstract

Sco X-1 is the brightest observed extrasolar X-ray source, which is a neutron star (NS) low-mass X-ray binary (LMXB) and is thought to have a strong potential for continuous gravitational waves (CW) detection due to its high accretion rate and relative proximity. Here, we compute the long-term evolution of its parameters, particularly the NS spin frequency (ν) and the surface magnetic field (B), to probe its nature and its potential for CW detection. We find that Sco X-1 is an unusually young ($\sim 7 \times 10^6$ yr) LMXB and constrain the current NS mass to $\sim$1.4–1.6 $M_\odot$. Our computations reveal a rapid B decay, with the maximum current value of $\sim 1.8 \times 10^8$ G, which can be useful to constrain the decay models. Note that the maximum current ν value is $\sim$550 Hz, implying that, unlike what is generally believed, a CW emission is not required to explain the current source properties. However, ν will exceed an observed cutoff frequency of $\sim$730 Hz, and perhaps even the NS breakup frequency, in the future without a CW emission. The minimum NS mass quadrupole moment (Q) to avoid this is $\sim(2\text{–}3) \times 10^{37}$ g cm^2, corresponding to a CW strain of $\sim 10^{-26}$. Our estimation of current ν values can improve the CW search sensitivity.

Unified Astronomy Thesaurus concepts: Gravitational waves (678); Neutron stars (1108); Low-mass x-ray binary stars (939); Accretion (14); X-ray binary stars (1811)

1. Introduction

A neutron star (NS) low-mass X-ray binary (LMXB) is a binary stellar system in which the NS accretes matter from a low-mass ($\lesssim 1.5 M_\odot$) donor or donor star (D. Bhattacharya & E. van den Heuvel 1991). The accretion happens when the donor fills its Roche lobe. Since this accreted matter has a large amount of specific angular momentum, it typically spins up the NS to a spin frequency (ν) of a few hundred Hz. When the accretion finally stops, i.e., at the end of the LMXB phase, such rapidly spinning NSs can manifest as radio millisecond pulsars (MSPs; B. Bhattacharyya & J. Roy 2022). Even in the LMXB phase, if the accretion disk is stopped by the NS magnetosphere, the disk matter may be channeled via accretion columns to the stellar magnetic poles. This can create azimuthally asymmetric emission from the spinning NS, and hence the observed X-ray emission can have periodic variation with the stellar spin frequency ν. Such systems are called accretion-powered millisecond X-ray pulsars (e.g., A. Patruno & A. L. Watts 2021; T. Di Salvo & A. Sanna 2022).

If a spinning NS is asymmetric around its spin axis, implying a nonzero ellipticity (ϵ) or mass quadrupole moment ($Q = I\epsilon$; I: NS moment of inertia), such an NS should emit gravitational waves continuously and spin down (S. L. Shapiro & S. A. Teukolsky 1983). Note that other physical mechanisms, such as r-mode instability and f-mode instability, etc., can also cause continuous gravitational wave (CW) emission from NSs (for a comprehensive review, see K. Glampedakis & L. Gualtieri 2018). While such CWs have not been detected so far and only upper limits of ϵ have been estimated for a number of NSs (e.g., B. P. Abbott et al. 2017, 2019; R. Abbott et al. 2020; L. Nieder et al. 2020, 2019; J. T. Whelan et al. 2023), such waves have been inferred from electromagnetic observations (e.g., S. Bhattacharyya & D. Chakrabarty 2017; B. Haskell & A. Patruno 2017; G. Woan et al. 2018; S. Bhattacharyya 2020). Studies of CWs from spinning NSs can be very useful to probe their physics, formation, and evolution, and hence the detection of CW is a holy grail of physics and astronomy.

What are the best sources to search for CW? Among NS LMXBs, Scorpius X-1 (Sco X-1) is thought to be a very promising source for CW detection (see A. Mukherjee et al. 2018; G. Pagliaro et al. 2023, and references therein) because of its relatively low distance ($d = 2.8$ kpc; C. F. Bradshaw et al. 1999) and a very high and persistent accretion rate $\dot{M}$ (of the order of $10^{-8} M_\odot$ yr^{-1}; D. Mata Sánchez et al. 2015; A. L. Watts et al. 2008). Here is the justification for the latter argument. Such a high $\dot{M}$ value could spin up the NS beyond the breakup ν ($\nu_{\rm break} \gtrsim 1200$ Hz; S. Bhattacharyya et al. 2016), which has not obviously happened. Even if the current ν ($=\nu_{\rm curr}$) for Sco X-1 does not exceed $\nu_{\rm break}$, it could exceed an observationally indicated upper cutoff of ν ($\sim$730 Hz; D. Chakrabarty et al. 2003; D. Chakrabarty 2008; A. Patruno 2010). These hint at a braking torque on the NS to keep its ν within a reasonable limit. CW can provide such a braking torque and cause the pulsar to spin down (e.g., S. Bhattacharyya & D. Chakrabarty 2017). However, in spite of this promise, the CW detection from Sco X-1 could be challenging and has not been detected yet in recent searches (Y. Zhang et al. 2021; R. Abbott et al. 2022a, 2022b; J. T. Whelan et al. 2023). This is because the source is not a pulsar, and hence the ν value is not known (see S. Galaudage et al. 2021 and references therein). Note that a known $\nu_{\rm curr}$ value reduces the volume of the parameter space and hence improves the sensitivity for CW searches. However, in the absence of a

measured $\nu_{\rm curr}$ value, one could estimate a range of $\nu_{\rm curr}$ values by the computation of the long-term evolution of the LMXB and reproducing other known source parameters (e.g., A. Kar et al. 2024). Some such parameter values of Sco X-1 are orbital period $P_{\rm orb} = 0.787$ days (L. Wang et al. 2018), donor-to-NS mass ratio $q = 0.52^{+0.16}_{-0.15}$ (L. Wang et al. 2018), accretion rate $\dot{M} = 2.2 \times 10^{-8}\, M_\odot\ {\rm yr}^{-1}$ (D. Mata Sánchez et al. 2015; A. L. Watts et al. 2008), and donor star temperature $T_{\rm donor} < 4800$ K (D. Mata Sánchez et al. 2015). Such a computation is also useful to probe the binary and stellar evolution and the NS physics and to estimate other unknown parameters, including Q or ϵ. However, while a few papers, such as W.-C. Chen (2017) and K. X. Van & N. Ivanova (2019), computed the binary evolution for Sco X-1 to match some observationally known values of parameters (e.g., $P_{\rm orb}$, q, $\dot{M}$, $T_{\rm donor}$) at the current time, they did not compute and constrain most NS parameters (e.g., ν, Q).

A. Kar et al. (2024) explored the NS LMXB evolution, including the evolution of NS and binary parameters, for ranges of initial and fixed parameter values. Using the methods outlined in that paper, here we compute the binary evolution for Sco X-1, and for the first time, calculate the ν evolution for this source considering different Q values. Note that, unlike some previous papers (e.g., Y. Zhang et al. 2021), we do not consider the special condition of a balance between the accretion torque and the CW torque. This condition, even if satisfied for certain periods, may not generally hold during the entire LMXB phase and hence might not be valid at the current time. This is because the mass transfer rate from the donor star evolves drastically throughout the LMXB phase (e.g., A. Kar et al. 2024), and the CW may not entirely depend on accretion (e.g., S. Bhattacharyya 2020). Therefore, we consider the general case of the mutually independent evolution of these torques depending on the evolution of various source parameter values. Our computations constrain some NS parameters, e.g., mass ($M_{\rm NS}$), ν, ϵ, and surface magnetic field (B), which, among various aspects, could be useful for future CW detection from Sco X-1.

2. Methods

We use Modules for Experiments in Stellar Astrophysics (MESA),[4] an open-source 1D stellar evolution code (B. Paxton et al. 2011, 2013, 2015, 2018, 2019), to compute the binary evolution for Sco X-1. The binary parameter evolution and the Roche Lobe overflow primarily depend on the angular momentum (J) loss from the system, and the magnetic braking (MB) is the dominant mechanism for such a loss for the donor star of Sco X-1 (K. X. Van & N. Ivanova 2019). However, a common prescription of MB (S. Rappaport et al. 1983) cannot reproduce the observed high accretion rate of Sco X-1, and hence we use the "Convection And Rotation Boosted" (CARB) prescription with the loss of J due MB given by (K. X. Van & N. Ivanova 2019)

$$\dot{J}_{\rm MB} = -\frac{2}{3}\dot{M}_{\rm W}^{-1/3} R^{14/3} (v_{\rm esc}^2 + 2\Omega^2 R^2/K_2^2)^{-2/3} \times \Omega_\odot\, B_\odot^{8/3} \left(\frac{\Omega}{\Omega_\odot}\right)^{11/3} \left(\frac{\tau_{\rm conv}}{\tau_{\odot,{\rm conv}}}\right)^{8/3}. \quad (1)$$

Here, $\dot{M}_{\rm W}$ represents wind mass-loss rate from donor star, R is the donor star radius, $v_{\rm esc}$ denotes surface escape velocity of the donor star, Ω is the rotation rate, K_2 represents the limit where the rotation rate has a significant role, and $\tau_{\rm conv}$ is convective turnover time. The other components of $\dot{J}$ due to gravitational radiation and mass loss are considered according to their standard prescription mentioned in earlier papers (e.g., K. Jia & X.-D. Li 2015; A. J. Goodwin & T. E. Woods 2020). However, although we primarily use the "CARB" MB prescription, we also run MESA, following the general results of H.-R. Yang & X.-D. Li (2024), for the "Convection Boosted" (CBOOST) MB scheme (Equation (20) of K. X. Van et al. 2019, with $\xi = 2$). For baryonic to gravitational mass conversion for the NS, we use Equation (19) of F. Cipolletta et al. (2015), as outlined in A. Kar et al. (2024). We calculate the NS radius as $R_{\rm NS} = A M_{\rm NS}^{1/3}$, where the value of the proportionality constant A has been determined by taking an NS radius of 11.2 km for the NS mass of $1.4\, M_\odot$.

In order to model the NS spin evolution, we follow the torque prescription in S. Bhattacharyya & D. Chakrabarty (2017) and references therein. The torques in the accretion and propeller phases ($N_{\rm acc}$ and $N_{\rm prop}$, respectively) are

$$N_{\rm acc} = \dot{M}\sqrt{GM_{\rm NS} r_{\rm m}} + \frac{\mu^2}{9 r_{\rm m}^3}\left[2\left(\frac{r_{\rm m}}{r_{\rm co}}\right)^3 - 6\left(\frac{r_{\rm m}}{r_{\rm co}}\right)^{\frac{3}{2}} + 3\right], \quad (2)$$

$$N_{\rm prop} = -\eta\dot{M}\sqrt{GM_{\rm NS} r_{\rm m}} - \frac{\mu^2}{9 r_{\rm m}^3}\left[3 - 2\left(\frac{r_{\rm co}}{r_{\rm m}}\right)^{3/2}\right], \quad (3)$$

where $r_{\rm m} (\propto B^{4/7}\dot{M}^{-2/7})$ and $r_{\rm co} (\propto \nu^{-2/3})$ are the magnetospheric radius and corotation radius, respectively (e.g., S. Bhattacharyya & D. Chakrabarty 2017), μ is the NS surface magnetic dipole moment, and η is a constant of the order of unity. In order to make our results realistic, we also consider that the NS surface magnetic field evolves as prescribed in N. Shibazaki et al. (1989):

$$B(t) = \frac{B_{\rm i}}{1 + \Delta M_{\rm acc}(t)/m_{\rm B}}, \quad (4)$$

where $B_{\rm i}$ is the initial NS surface magnetic field, $B(t)$ is the NS surface magnetic field at time t after the accretion of $\Delta M_{\rm acc}(t)$ mass, and $m_{\rm B}$ is a constant mass that determines the decay rate of the magnetic field. The current value of the NS magnetic field is $B_{\rm curr}$.

Sco X-1 does not show pulsations (see Section 1), and it is clearly in the accretion phase (i.e., $r_{\rm m} \leqslant r_{\rm co}$; S. Bhattacharyya & D. Chakrabarty 2017) with a high accretion rate (see Figure 1). Hence, at the current time, the NS magnetic field may be too weak to stop the accretion disk and cannot channel the accreted matter to the magnetic poles (see Section 1). Therefore, we consider that the accretion disk inner radius is currently either $R_{\rm NS}$ or $r_{\rm ISCO}$ (ISCO: innermost stable circular orbit), whichever is greater (i.e., $\max[R_{\rm NS}, r_{\rm ISCO}]$; $r_{\rm ISCO} (= 6GM/c^2)$, G: gravitational constant, c: speed of light in vacuum). Thus, at the current time, the lack of pulsations in the accretion phase implies that $r_{\rm m} \not> \max[R_{\rm NS}, r_{\rm ISCO}]$, and there is no significant disk–magnetosphere interaction. Consequently, we consider $N_{\rm acc} = \dot{M}\sqrt{GM_{\rm NS}\max[R_{\rm NS}, r_{\rm ISCO}]}$ (from Equation (2)) for the current time.

[4] https://docs.mesastar.org/en/release-r23.05.1/

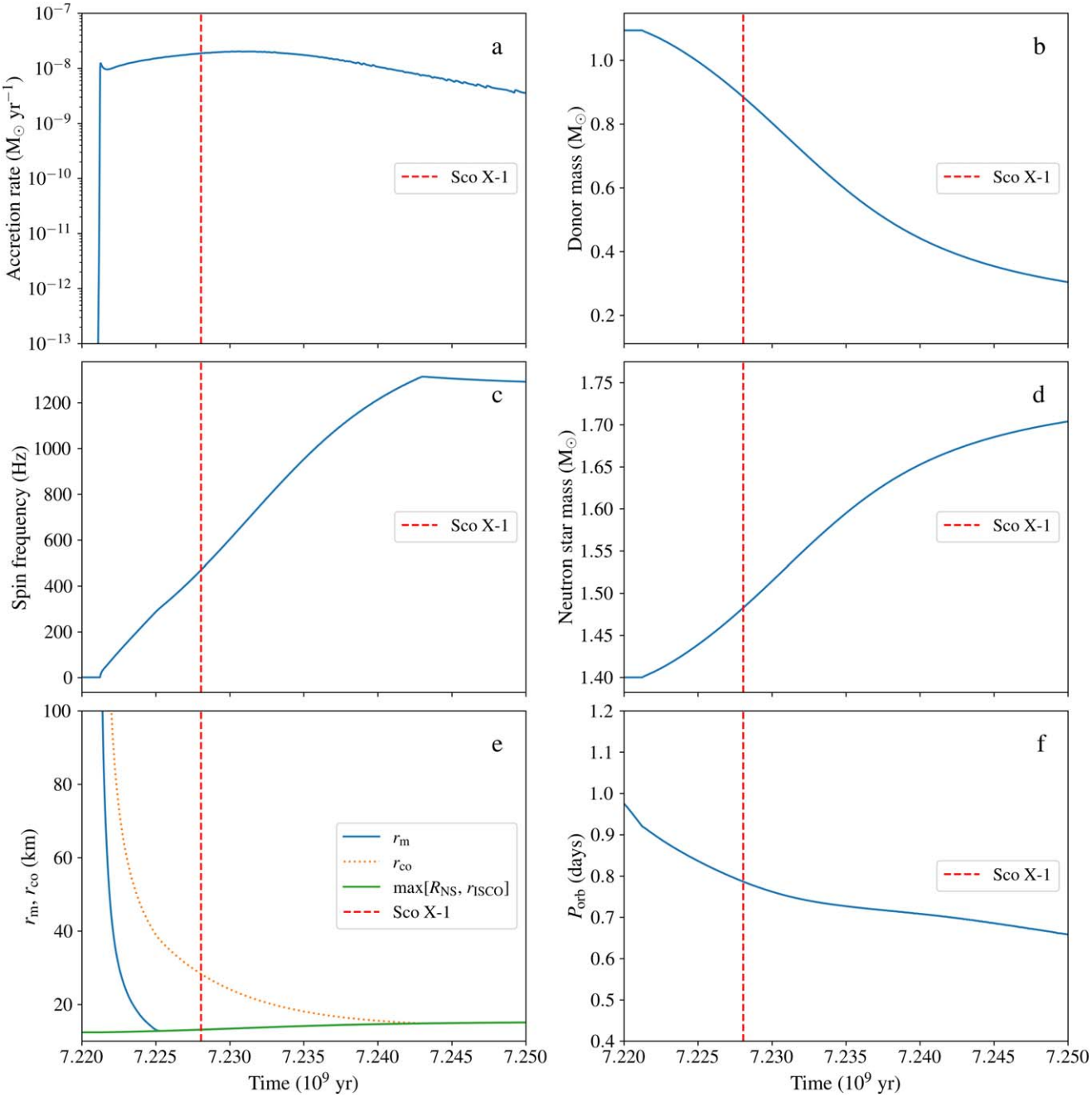

Figure 1. Evolution of parameters (accretion rate (panel (a)), donor star mass (panel (b)), NS spin frequency (panel (c)), NS mass (panel (d)), characteristic radii (panel (e)), and binary orbital period (panel (f))) for our best model of Sco X-1 evolution as computed using MESA (Section 3). The initial magnetic field (B_i) is taken to be 6×10^{11} G with $m_B = 1 \times 10^{-5}$. The dashed vertical line shows the time at which all the observed parameters of Sco X-1—P_{orb}, $\dot{M}$, q, and T_{donor}—match. The time mentioned on the x-axis is calculated from the start of the binary evolution computation.

For the $Q > 0$ cases, we use the following CW torque (L. Bildsten 1998):

$$N_{CW} = -\frac{32GQ^2}{5}\left(\frac{2\pi\nu}{c}\right)^5. \quad (5)$$

In order to calculate the CW strain (which is crucial for CW detection), we use the equation (M. Zimmermann & E. Szedenits 1979; K. Glampedakis & L. Gualtieri 2018):

$$h_0 = \frac{4\pi^2 GI}{c^4 d} f_{CW}^2 \epsilon, \quad (6)$$

where f_{CW} is the frequency of CW taken to be 2ν.

3. Results

We consider ranges of values for initial and fixed parameters (e.g., A. Kar et al. 2024), such as donor star mass (M_{donor}), M_{NS}, P_{orb}, fractional loss of the mass transferred from the donor star (β), and irradiation efficiency (ϵ_{irr}), for our MESA evolution models. K. X. Van & N. Ivanova (2019) found that the reproduction of observed Sco X-1 parameter values requires a narrow initial parameter space. Motivated by this, we consider initial ranges of M_{donor} (1.0–1.2 $M_\odot$), P_{orb} (2.75–2.82 days), M_{NS} (1.35–1.6 $M_\odot$), and also a range (0.3–0.7) of β for our computation. When we study the effects of change of one parameter value, we fix the other parameters at their canonical

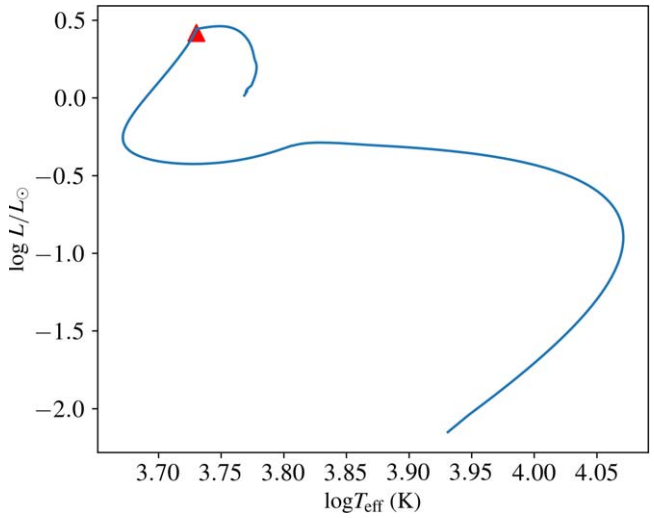

Figure 2. The H-R diagram for the donor star evolution (starting from the upper end) of Sco X-1, as computed with MESA. The initial parameter values are for the best model mentioned in Section 3. The current position of the source is depicted by a red triangle.

values (e.g., $M_{\rm NS} = 1.4\,M_\odot$, $M_{\rm donor} = 1.1\,M_\odot$, $P_{\rm orb} = 2.80$ days, $\beta = 0.5$). Note that the values of parameters, such as $\epsilon_{\rm irr}$ and η, do not have visible effects for our computation to reproduce Sco X-1 parameter values. By exploring the MESA evolution within the abovementioned ranges, we find that the model with initial $P_{\rm orb} = 2.8$ days and initial $M_{\rm donor} = 1.1\,M_\odot$ reproduces the observed parameter values closely (Figure 1). We match the observed values of $P_{\rm orb}$, q, and $\dot{M}$ within 1% and $T_{\rm donor}$ within <5%. From this best model, we get $\dot{M} = 1.92 \times 10^{-8}\,M_\odot\ {\rm yr}^{-1}$, $P_{\rm orb} = 0.786$ days, $q = 0.596$, and $T_{\rm donor} \sim 5000$ K, all of which match most closely with the observed ranges of parameter values for Sco X-1 mentioned in Section 1. From the evolution, it can be seen that the accretion starts at $\sim 7.22 \times 10^9$ yr (Figure 1). Moreover, note that the best model implies a current value of $M_{\rm NS}$ of $\sim 1.48\,M_\odot$, and considering all reasonably matching evolution models, the current $M_{\rm NS}$ range is ~ 1.42–$1.6\,M_\odot$. Figure 2 shows the Hertzsprung–Russell (H-R) diagram of the evolution of the donor star of Sco X-1 and its current position.

With our best model, we calculate the spin evolution and estimate the current ν value ($\nu_{\rm curr}$) of Sco X-1 (see A. Kar et al. 2024 and Section 2 for details). For the default model, we keep $Q = 0$, i.e., we take a case without CW. However, with the usually considered value of $m_{\rm B}$ ($\sim 10^{-4}\,M_\odot$; N. Shibazaki et al. 1989) in Equation (4), we cannot satisfy the condition of no pulsation in the accretion phase, i.e., $r_{\rm m} \not> \max[R_{\rm NS}, r_{\rm ISCO}]$ (see Section 2). Hence, we explore a range of lower $m_{\rm B}$ values, which allows a faster decay of NS magnetic field (Figure 3) and, in turn, provides lower $B_{\rm curr}$ values resulting in lower $r_{\rm m}$ values (e.g., S. Bhattacharyya & D. Chakrabarty 2017). We assume a reasonable lower limit of $B_{\rm curr}$ ($\sim 10^7$ G; see D. Mukherjee et al. 2015).

The conditions $r_{\rm m} \not> \max[R_{\rm NS}, r_{\rm ISCO}]$ and $B_{\rm curr} \gtrsim 10^7$ G provide a range of $m_{\rm B}$ for each $B_{\rm i}$. We consider a reasonable $B_{\rm i}$ range of 6×10^{11}–2×10^{12} G (e.g., D. Bhattacharya & E. van den Heuvel 1991). This provides an overall range of $m_{\rm B}$ ($\sim 6 \times 10^{-7}$–2.5×10^{-5}; for our best model; Table 1). Note that, due to the above two conditions, $B_{\rm curr}$ has a similar range for all $B_{\rm i}$ values (upper value of $B_{\rm curr} \sim 1.8 \times 10^8$ G; see Table 1, for example). Moreover, as indicated above, a lower

Table 1
Several Example Initial Magnetic Field ($B_{\rm i}$) Values and Their Corresponding $m_{\rm B}$, Current Magnetic Field ($B_{\rm curr}$), and Current Spin Frequency ($\nu_{\rm curr}$) Ranges for Sco X-1 Using Evolution Computations with MESA (for No CW; Sections 2 and 3)

$B_{\rm i}$ (G)	$m_{\rm B}$	$B_{\rm curr}$ (G)	$\nu_{\rm curr}$ (Hz)
6×10^{11}	2.5×10^{-5}	1.81×10^8	539.8
	8×10^{-6}	5.8×10^7	451.8
	5×10^{-6}	3.62×10^7	419.8
	2×10^{-6}	1.45×10^7	375.7
8×10^{11}	1.8×10^{-5}	1.74×10^8	537.7
	8×10^{-6}	7.74×10^7	474.6
	4×10^{-6}	3.87×10^7	423.6
	1.5×10^{-6}	1.45×10^7	375.7
1×10^{12}	1.5×10^{-5}	1.81×10^8	539.8
	8×10^{-6}	9.67×10^7	492.2
	4×10^{-6}	4.83×10^7	438.6
	1.2×10^{-6}	1.45×10^7	375.7
2×10^{12}	7.5×10^{-6}	1.81×10^8	539.7
	4×10^{-6}	9.67×10^7	492.3
	1×10^{-6}	2.41×10^7	397.2
	6×10^{-7}	1.45×10^7	375.6

$m_{\rm B}$ value implies a lower $B_{\rm curr}$ value (Table 1 and Figure 3). Besides, as B decays faster for a lower $m_{\rm B}$ value, the spin-up torque also decreases faster (see Section 2; Equation (2)), and hence the spin-up rate is slower. Therefore, at a given time (e.g., the current time), ν is lower for lower $m_{\rm B}$ and B values (see Table 1 and Figure 3). However, as the range of $B_{\rm curr}$ does not depend on $B_{\rm i}$, the range of $\nu_{\rm curr}$ ($\sim$370–540 Hz for the best model) also does not depend on $B_{\rm i}$ (Table 1 and Figure 3). Furthermore, we consider other evolution models, which reasonably match the Sco X-1–observed parameter values, and get similar ranges of $m_{\rm B}$, $B_{\rm curr}$, and $\nu_{\rm curr}$, as mentioned above. From all of these models combined, $\nu_{\rm curr}$ comes out to be $\sim$350–550 Hz.

Let us now consider the effects of CW ($Q > 0$) on the NS spin evolution for Sco X-1. For the LMXB phase and the radio MSP phase (Section 1), $\epsilon \sim 10^{-9}$ or $Q \sim 10^{36}$ g cm^2 for NSs has been inferred using electromagnetic observations (e.g., G. Woan et al. 2018; S. Bhattacharyya 2020). Nevertheless, we explore a Q range of $\sim 10^{36-38}$ g cm^2 ($\epsilon \sim 10^{-9}$–10^{-7}) and even higher.

The effects of Q on the NS spin evolution for Sco X-1 are shown in Figure 4. Here, we consider a Q range of $\sim 10^{36-38}$ g cm^2, where the lower Q values are motivated by S. Bhattacharyya (2020). Note that $Q \geqslant 2.3 \times 10^{37}$ g cm^2 for our best model (Section 3), $B_{\rm i} = 6 \times 10^{11}$ G and $m_{\rm B} = 2.5 \times 10^{-5}$ imply that ν did not and will not exceed the observationally indicated upper cutoff of ν (~ 730 Hz; Section 1) throughout the LMXB phase of Sco X-1. This minimum Q is called $Q_{\rm min(730)}$ for the abovementioned model. If we consider a very high value of Q (e.g., 10^{40} g cm^2) as the $Q_{\rm max}$, then the allowed $\nu_{\rm curr}$ range for $Q_{\rm min(730)} - Q_{\rm max}$ for the abovementioned model is $\sim$500–70 Hz (Figure 4). For all the matching evolution models and the allowed $m_{\rm B}$ range for Sco X-1, the allowed $\nu_{\rm curr}$ range for $Q_{\rm min(730)} - Q_{\rm max}$ is $\sim$510–60 Hz. However, for a Q range of $0 - Q_{\rm max}$, the range of $\nu_{\rm curr}$ for all matching models is $\sim$550–60 Hz.

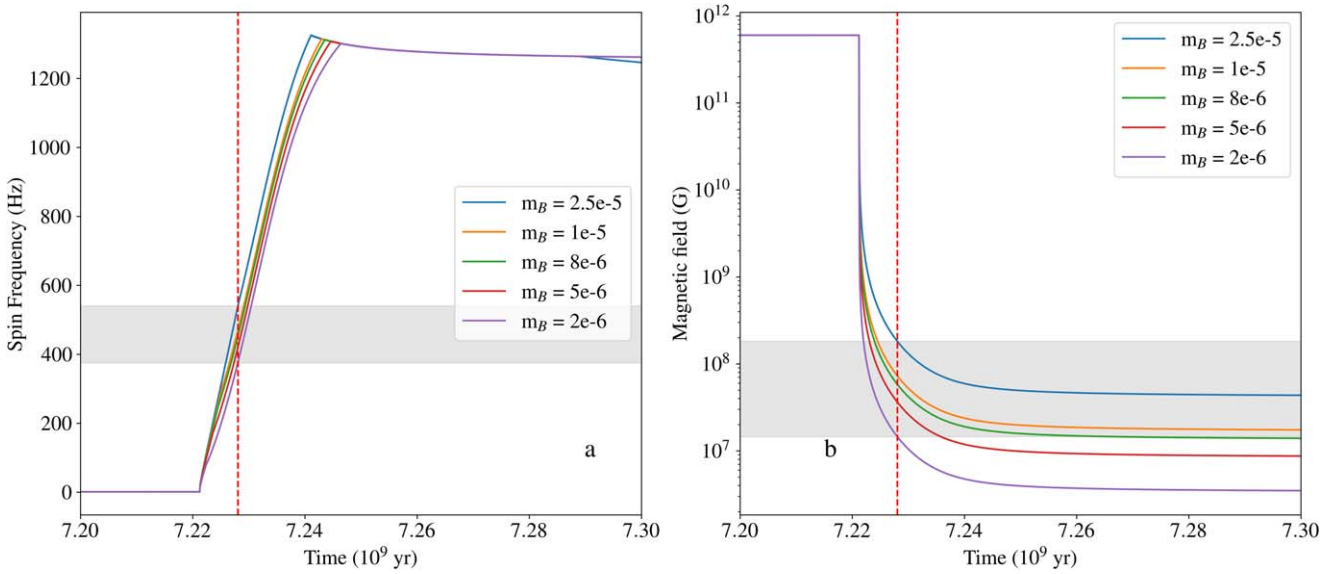

Figure 3. The evolution of the spin frequency (ν) (panel (a)) and the surface magnetic field (B) (panel (b)) of the NS of Sco X-1 for different values of m_B (Equation (4)) considering the best model mentioned in Section 3. The time mentioned on the x-axis is calculated from the start of the binary evolution computation. The accretion starts at $\sim 7.22 \times 10^9$ yr, which is evident from the steep rise of the ν-curve from its initial flat trajectory. The initial B is assumed to be $=6 \times 10^{11}$ G. The dashed vertical line shows the time at which all the observed parameters of Sco X-1—$P_{\rm orb}$, $\dot{M}$, q, and $T_{\rm donor}$—match. The gray patches indicate the allowed ranges of the current $\nu(=\nu_{\rm curr})$ and $B(=B_{\rm curr})$ for the m_B values considered (see Section 3).

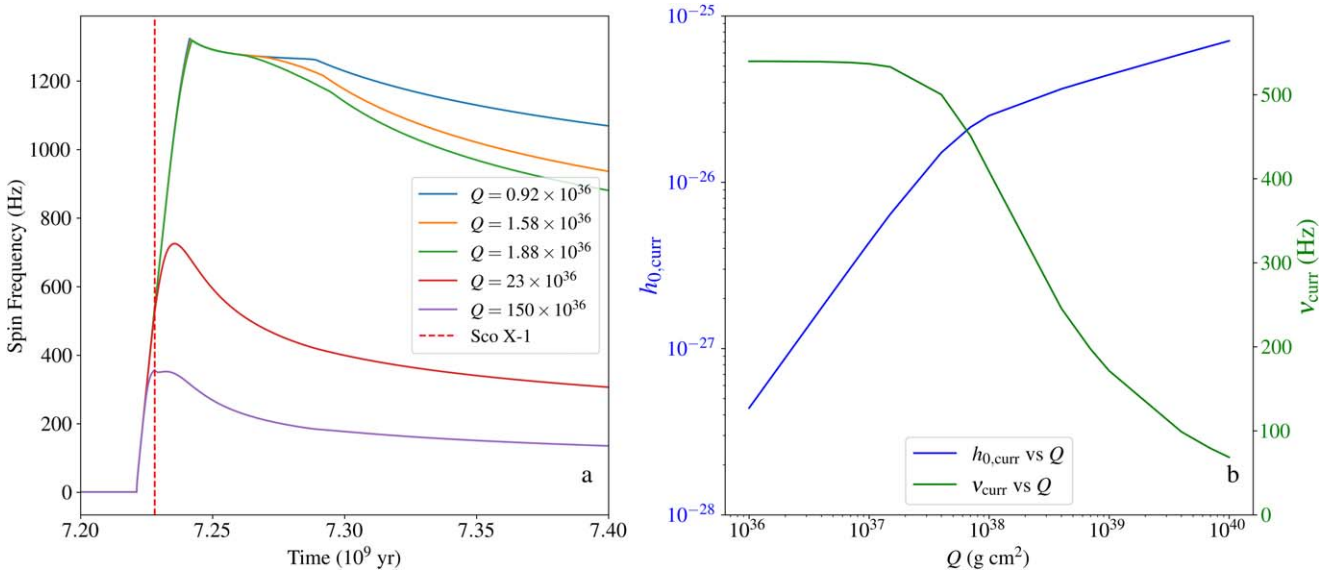

Figure 4. Panel (a): the evolution of the NS spin frequency (ν) for Sco X-1 for different values of Q (Equation (5)) considering the best model mentioned in Section 3. The time mentioned on the x-axis is calculated from the start of the binary evolution computation. The $B_{\rm i}$ and m_B values are 6×10^{11} G and 2.5×10^{-5}, respectively. The dashed vertical line shows the time at which all the observed parameters of Sco X-1—$P_{\rm orb}$, $\dot{M}$, q, and $T_{\rm donor}$—match. Panel (b): the CW strain amplitude $h_{0,\rm curr}$ and the NS spin frequency $\nu_{\rm curr}$ for Sco X-1 at the current time for a range of Q values (for the abovementioned best model, $B_{\rm i}$, and m_B values; Section 3). Note that $h_{0,\rm curr}$ increases slowly beyond $Q \sim 10^{38}$ g cm^2 ($\epsilon \sim 10^{-7}$).

We calculate the current CW strain, $h_{0,\rm curr}$, as a function of Q for Sco X-1 using Equation (6). In order to constrain $h_{0,\rm curr}$, we plot $h_{0,\rm curr}$ versus Q in Figure 4(b). In the same panel, we also plot $\nu_{\rm curr}$ versus Q. Let us understand these two curves. As one gradually considers higher Q values starting from a low value, initially $\nu_{\rm curr}$ does not decrease much when the Q values are still small (as $N_{\rm CW} \propto Q^2$; Equation (5)). Consequently, $h_{0,\rm curr}$ increases rapidly with Q (roughly proportionally; Equation (6); see Figure 4(b)). But, for larger Q values ($\gtrsim 10^{38}$ g cm^2), $\nu_{\rm curr}$ decreases rapidly (as $N_{\rm CW} \propto Q^2$; Equation (5)). As a result, $h_{0,\rm curr}$ increases slowly with Q because $h_{0,\rm curr} \propto \nu_{\rm curr}^2 Q$ (Equation (6)). This means, even if the Q value of the NS in Sco X-1 is much larger than $\sim 10^{38}$ g cm^2, the $h_{0,\rm curr}$ value is not significantly greater than the value for $Q \sim 10^{38}$ g cm^2. In fact, we do not expect an $h_{0,\rm curr}$ value greater than a few times 10^{-26} (see Figure 4(b)). This points to the requirement of a minimum instrument capability for the CW detection from Sco X-1.

For the models with the MB prescription "CBOOST" (see Section 2), we use the similar initial parameter values around the mentioned ranges for the "CARB" model. With this prescription too, the observed parameter values for Sco X-1 can

be closely matched, except for $P_{\rm orb}$, which could be matched within ∼20% at the best. The NS parameter (such as ν, $B_{\rm curr}$) values calculated for "CBOOST" are similar to those obtained for the "CARB" models. For example, $\nu_{\rm curr}$ values are within the range of ∼300–600 Hz, which overlap with the range obtained for"CARB."

4. Discussion and Conclusion

Sco X-1 is the first discovered and the brightest observed extrasolar X-ray source. This persistent source is thought to be among the best potential sources to detect CWs (Section 1). Here, we compute the long-term evolution of this source to understand its nature and its potential for CW detection. Our computation of evolution of Sco X-1 using the MESA code shows that it is an unusually young NS LMXB (age $\sim 7 \times 10^6$ yr) with a predicted total LMXB lifetime of $\sim 5 \times 10^8$ yr, which is also surprisingly short (see Appendix). The LMXB phase ends when the donor star does not fill its Roche lobe anymore. Moreover, the current accretion rate of the NS of Sco X-1 is rather high, which cannot be explained with a usual MB prescription and requires a boosted braking prescription, such as "CARB" or "CBOOST." While our evolution computations reproduce the known parameter values of Sco X-1, we could also constrain the current NS mass to the range ∼1.42–1.6 $M_\odot$ (Section 3). Note that mass measurement of an NS is important to probe the nature of the degenerate NS core matter at supranuclear densities (S. Bhattacharyya 2010).

We compute the NS spin frequency ν and surface magnetic field B evolution for Sco X-1 for the first time to the best of our knowledge. Here, we utilize the lack of observed pulsations from this source (see Sections 1 and 2) for the first time. We find that the maximum value of the current B, i.e., of $B_{\rm curr}$, is $\sim 1.8 \times 10^8$ G. Thus, it is remarkable that the B value of the NS decays by at least ∼4 orders of magnitude in just ∼7 million years, and this fast B decay is also supported by our preferred low $m_{\rm B}$ values (Section 3). Note that the physics of the B decay of NSs is a topical problem of astrophysics (A. P. Igoshev et al. 2021), and our finding should be important to constrain models. For example, the high $\dot{M}$ could screen the magnetic field lines so well that they could not reemerge easily. Alternatively, the ohmic decay could be more efficient due the high temperature because of the high $\dot{M}$. It is important to note that, even without CWs, the current ν, i.e., $\nu_{\rm curr}$, value is not more than ∼550 Hz (Section 3). This value is well below both the breakup ν and the observed cutoff ν (see Section 1). This means that the CW from Sco X-1 is not required, considering its current properties. Hence, unlike what is usually believed (see Section 1), the current high $\dot{M}$ of this source does not need CWs, and hence Sco X-1 might not be one of the best sources for CW detection. Nevertheless, the source could still emit CWs, and considering a Q value up to $\sim 10^{40}$ g cm^2, the lower limit of $\nu_{\rm curr}$ could be ∼60 Hz. Note that our estimation of $\nu_{\rm curr}$ values as a function of Q can be very useful to improve the sensitivity for CW searches (see Section 1). However, our evolution computations show that the ν value will exceed ∼1200 Hz in the future if no CW is considered (see Appendix). Thus, if we assume that ν will not exceed the observed cutoff ν (see Section 1) even in the future, then we need a Q of at least $\sim(2–3) \times 10^{37}$ g cm^2, implying a current CW strain h_0, i.e., $h_{0,\rm curr}$, of $\sim 10^{-26}$ (see Section 3, Figure 4(b)). However, even for a very high $Q \sim 10^{40}$ g cm^2 (i.e., $\epsilon \sim 10^{-5}$), $h_{0,\rm curr}$ would not be more than $\sim 7 \times 10^{-26}$ (see Section 3, Figure 4(b)). These upper limits on $h_{0,\rm curr}$ are somewhat comparable to those obtained from the Advanced LIGO data (e.g, B. P. Abbott et al. 2017; J. T. Whelan et al. 2023).

Appendix

Here, we show, in Figure A1, the evolution of some parameters performed by the MESA code (see Section 2), for the entire LMXB phase of Sco X-1. This is useful to understand the nature of this source and, thus, to provide a broad and general perspective of our results and conclusions.

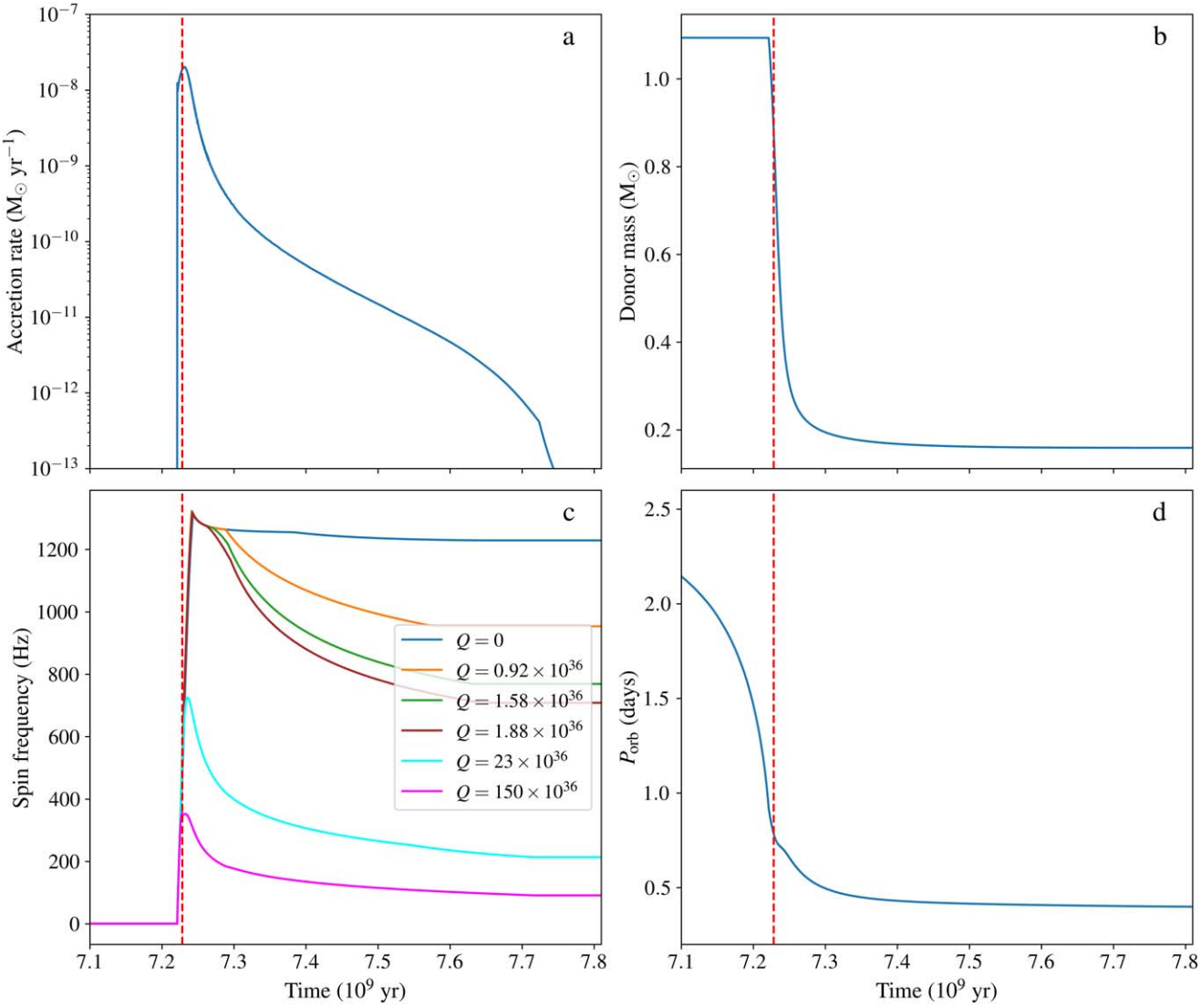

Figure A1. Evolution of parameter values, accretion rate (panel (a)), donor star mass (panel (b)), NS spin frequencies (ν for various Q values; panel (c)), and binary orbital period (P_{orb}; panel (d)) during the entire LMXB phase for the best model of Sco X-1 (see Section 3). B_i and m_B values are 6×10^{11} G and 2.5×10^{-5}, respectively. The time mentioned on the x-axis is calculated from the start of the binary evolution computation, and the dashed vertical line shows the time at which all the observed parameters of Sco X-1—P_{orb}, $\dot{M}$, q, and T_{donor}—match. This figure shows that Sco X-1 is a relatively young NS LMXB, and its LMXB phase will be relatively short-lived.

ORCID iDs

Abhijnan Kar https://orcid.org/0000-0001-9207-7803
Sudip Bhattacharyya https://orcid.org/0000-0002-6351-5808

References

Abbott, B. P., Abbott, R., Abbott, T. D., et al. 2017, ApJ, 847, 47
Abbott, B. P., Abbott, R., Abbott, T. D., et al. 2019, ApJ, 879, 10
Abbott, R., Abbott, T. D., Abraham, S., et al. 2020, ApJL, 902, L21
Abbott, R., Abe, H., Acernese, F., et al. 2022a, PhRvD, 106, 062002
Abbott, R., Abe, H., Acernese, F., et al. 2022b, ApJL, 941, L30
Bhattacharya, D., & van den Heuvel, E. 1991, PhR, 203, 1
Bhattacharyya, B., & Roy, J. 2022, in Millisecond Pulsars, ed. S. Bhattacharyya, A. Papitto, & D. Bhattacharya (Cham: Springer), 1
Bhattacharyya, S. 2010, AdSpR, 45, 949
Bhattacharyya, S. 2020, MNRAS, 498, 728
Bhattacharyya, S., Bombaci, I., Logoteta, D., & Thampan, A. V. 2016, MNRAS, 457, 3101
Bhattacharyya, S., & Chakrabarty, D. 2017, ApJ, 835, 4
Bildsten, L. 1998, ApJL, 501, L89
Bradshaw, C. F., Fomalont, E. B., & Geldzahler, B. J. 1999, ApJL, 512, L121
Chakrabarty, D. 2008, in AIP Conf. Proc. 1068, A Decade of Accreting Millisecond X-ray Pulsars, ed. R. Wijnands et al. (Melville, NY: AIP), 67
Chakrabarty, D., Morgan, E. H., Muno, M. P., et al. 2003, Natur, 424, 42
Chen, W.-C. 2017, A&A, 606, A60
Cipolletta, F., Cherubini, C., Filippi, S., Rueda, J. A., & Ruffini, R. 2015, PhRvD, 92, 023007
Di Salvo, T., & Sanna, A. 2022, in Millisecond Pulsars, ed. S. Bhattacharyya, A. Papitto, & D. Bhattacharya (Cham: Springer), 87
Galaudage, S., Wette, K., Galloway, D. K., & Messenger, C. 2021, MNRAS, 509, 1745
Glampedakis, K., & Gualtieri, L. 2018, in The Physics and Astrophysics of Neutron Stars, ed. L. Rezzolla et al. (Cham: Springer), 673
Goodwin, A. J., & Woods, T. E. 2020, MNRAS, 495, 796
Haskell, B., & Patruno, A. 2017, PhRvL, 119, 161103
Igoshev, A. P., Popov, S. B., & Hollerbach, R. 2021, Univ, 7, 351
Jia, K., & Li, X.-D. 2015, ApJ, 814, 74
Kar, A., Ojha, P., & Bhattacharyya, S. 2024, MNRAS, 535, 344
Mata Sánchez, D., Muñoz-Darias, T., Casares, J., et al. 2015, MNRAS: Lett., 449, L1
Mukherjee, A., Messenger, C., & Riles, K. 2018, PhRvD, 97, 043016
Mukherjee, D., Bult, P., vanderKlis, M., & Bhattacharya, D. 2015, MNRAS, 452, 3994
Nieder, L., Clark, C. J., Bassa, C. G., et al. 2019, ApJ, 883, 42
Nieder, L., Clark, C. J., Kandel, D., et al. 2020, ApJL, 902, L46

Pagliaro, G., Papa, M. A., Ming, J., et al. 2023, ApJ, 952, 123
Patruno, A. 2010, ApJ, 722, 909
Patruno, A., & Watts, A. L. 2021, in Timing Neutron Stars: Pulsations, Oscillations and Explosions, ed. T. M. Belloni, M. Méndez, & C. Zhang (Berlin: Springer), 143
Paxton, B., Bildsten, L., Dotter, A., et al. 2011, ApJS, 192, 3
Paxton, B., Cantiello, M., Arras, P., et al. 2013, ApJS, 208, 4
Paxton, B., Marchant, P., Schwab, J., et al. 2015, ApJS, 220, 15
Paxton, B., Schwab, J., Bauer, E. B., et al. 2018, ApJS, 234, 34
Paxton, B., Smolec, R., Schwab, J., et al. 2019, ApJS, 243, 10
Rappaport, S., Verbunt, F., & Joss, P. C. 1983, ApJ, 275, 713
Shapiro, S. L., & Teukolsky, S. A. 1983, Black Holes, White Dwarfs, and Neutron Stars: The Physics of Compact Objects (New York: Wiley), 466
Shibazaki, N., Murakami, T., Shaham, J., & Nomoto, K. 1989, Natur, 342, 656
Van, K. X., & Ivanova, N. 2019, ApJL, 886, L31
Van, K. X., Ivanova, N., & Heinke, C. O. 2019, MNRAS, 483, 5595
Wang, L., Steeghs, D., Galloway, D. K., Marsh, T., & Casares, J. 2018, MNRAS, 478, 5174
Watts, A. L., Krishnan, B., Bildsten, L., & Schutz, B. F. 2008, MNRAS, 389, 839
Whelan, J. T., Tenorio, R., Wofford, J. K., et al. 2023, ApJ, 949, 117
Woan, G., Pitkin, M. D., Haskell, B., Jones, D. I., & Lasky, P. D. 2018, ApJL, 863, L40
Yang, H.-R., & Li, X.-D. 2024, ApJ, 974, 298
Zhang, Y., Papa, M. A., Krishnan, B., & Watts, A. L. 2021, ApJL, 906, L14
Zimmermann, M., & Szedenits, E. 1979, PhRvD, 20, 351